Corrosion behavior of Cr electrodeposited from Cr(VI) and Cr(III)-baths using direct (DCD) and pulse electrodeposition (PED) techniques

G. Saravanan, S. Mohan *

Central Electrochemical Research Institute, Karaikudi 630006, India

ABSTRACT

A comparison was made between the electrochemical corrosion behaviors of chromium deposited from hexavalent [Cr(VI)] and trivalent [Cr(III)] chromium baths using direct current (DCD) and pulse electro deposited (PED) techniques. Chromium coatings were deposited on mild-steel (MS) substrate. The corrosion behavior of both DCD and PED chromium from Cr(VI) and Cr(III)-baths in 3.5%NaCl solution was studied using potentiodynamic polarization and electrochemical impedance spectroscopy (EIS). The results indicated that PED chromium from Cr(VI) and Cr(III)-baths have higher charge-transfer resistance R_{ct} and very low I_{corr} than that of DCD chromium on mild-steel substrate.

© 2008 Elsevier Ltd. All rights reserved.

1. Introduction

Hexavalent chromium [Cr(VI)] plating has been commercialized many years before. A Cr(VI) plating bath operates at an elevated temperature and produces a mist of chromic acid. Since Cr(VI) plating produces hazardous air emissions, all Cr(VI) electro depositors must control and monitor the bath surface tension periodically. Cr(VI) widely recognized as a human carcinogen was reported to cause increased incidences of lung cancer. A United States Environmental Protection Agency (EPA) report [1] implicates Cr(VI) as a Group A known human carcinogen. The EPA also found that Cr(III) is much less toxic, classifies as a Group D carcinogen not classifiable as to carcinogenicity in humans. Cr(III) is rather insoluble and does not oxidize organic materials, poorly absorbed from gastrointestinal tract and is not considered to be a carcinogen. Cr(VI) is very reactive and causes ulceration of nasal septum and other tissues upon exposure as well as reproductive and gastrointestinal effects. The use of Cr(III) in industrial and commercial processes is preferred over Cr(VI) on the basis of comparison of the toxicities. Chromium is used in industry because of its excellent wear, corrosion resistance and attractive appearance [2,3]. The main advantage of Cr(III) plating bath in comparison with a Cr(VI)-bath is that Cr^{3+} ions are nontoxic environmentally benign [4]. However, it is almost impossible to deposit the Cr coating from a simple aqueous Cr(III) solution due to a very stable $[Cr(H_2O)_6]^{3+}$ complex [5]. According to the published data [6] the slow deposition rate in Cr(III) chloride electrolyte is related to the appearance of very

stable μ-hydroxo-bridged oligomeric species of Cr(III). To destabilize the strong hexa-aqua chromium(III) complex, some of the complexing agents (glycine, urea, dimethyl formamide, formic acid, acetate, sodium citrate, DL-aspartic acid, etc) may be used [7–11]. Chromium plating from Cr(VI) solution is now under scrutiny due to its toxicity and carcinogenicity; therefore, significant efforts have been applied to the development of alternative process for chromium plating from Cr(VI) solution [12]. The present work was important in terms of a Cr(VI)-free process, using Cr(III)-glycine solution as an alternate bath. Therefore, in the present work the aim was to compare the DC and PE-deposited chromium using a Cr(III)-glycine bath with Cr(VI)-bath. The microstructure and corrosion behavior were analyzed in 3.5%NaCl solution using potentiodynamic polarization and EIS.

2. Experimental

2.1. Materials preparation

Chromium coatings were electrochemically deposited from Cr(VI)-bath consisting of 250 g/L CrO_3, 2.5 g/L H_2SO_4 and Cr(III)-bath consisting of 212 g/L $CrCl_3 6H_2O$, 26 g/L NH_4Cl, 36 g/L NaCl, 20 g/L $B(OH)_3$, 75 g/L glycine and 200 ml methanol. AR grade chemicals and double distilled water were used to prepare the solution. The coatings were deposited on polished and electro-cleaned substrate of mild steel. The pH value of 2 ± 0.2 was maintained for Cr(III)-bath and stirred by mechanical stirrer. Graphite and lead were used as the anode for Cr(III) and Cr(VI)-baths, mild-steel plates were used as the cathode. The samples obtained

* Corresponding author. Tel.: +91 4565 227551; fax: +91 4565 227713.
E-mail address: sanjnamohan@yahoo.com (S. Mohan).

Table 1
Pulse parameter used for pulse plating of chromium.

Duty cycle (%)	Pulse frequency and pulse on-off times (ms)				Current density (A/dm^2)			
	10 Hz	25 Hz	50 Hz	100 Hz	Cr(III)-bath		Cr(VI)-bath	
					Peak	Average	Peak	Average
10	10–90	4–36	2–18	1–9	104	10.4	200	20
20	20–80	8–32	4–16	2–8	52	10.4	100	20
40	40–60	16–24	8–12	4–6	26	10.4	50	20
80	80–20	32–8	16–4	8–2	13	10.4	25	20

for mild steel, DC and PE-deposited chromium from Cr(VI) and Cr(III) were represented by (MS), Cr-(DCD)/MS from Cr(VI)-bath, Cr-(DCD)/MS from Cr(III)-bath, Cr-(PED)/MS from Cr(VI)-bath, and Cr-(PED)/MS from Cr(III)-bath, respectively. Pulse plating was done using Dynatronix (USA) DPR20-10-5 Model. The pulse parameters used are given in Table 1 [13]. The formula used in pulse plating is given below

$$\%\text{Duty cycle} = \frac{\text{ON time}}{\text{ON time} + \text{OFF time}} \times 100$$

$$\text{Average current} = \frac{\text{ON time}}{\text{Total time}} \times \text{peak pulse current}$$

$$\text{Peak current} = \frac{\text{Average current}}{\text{Duty cycle}} \times 100$$

The surface morphologies of the electrodeposits were characterized by SEM, and grain size and texture were assessed by X-ray diffraction (XRD) technique.

2.2. Corrosion measurements

2.2.1. Cell apparatus

Corrosion measurements were performed in a three-electrode cell with the volume of 150 mL. The samples (MS), Cr-(DCD)/MS from Cr(VI)-bath, Cr-(DCD)/MS from Cr(III)-bath, Cr-(PED)/MS from Cr(VI)-bath, and Cr-(PED)/MS from Cr(III)-bath were used as the working electrodes (WE). A platinum foil and a saturated calomel electrode (SCE) were used as the auxiliary electrode and reference electrode, respectively. The electrodes were connected to a potentiostate (PARSTAT 2273). The corrosion resistance parameters were obtained with inbuilt software package (powerCORR). All potentials in this work are referred to SCE.

2.2.2. Electrochemical procedures

Corrosion behavior was examined in neutral 3.5%NaCl solution at 30 ± 1 °C. Potentiodynamic polarization curves were measured for all the samples between −0.9 and −0.2 V at a scan rate of 5 mV/s. Impedance spectra were conducted at open circuit potential over a frequency range from 10^5 Hz to 10^{-2} Hz. The amplitude of potential modulation was 5 mV. All the recorded impedance spectra were shown as Bode and Nyquist diagrams.

3. Results and discussion

3.1. Microstructural characteristics

The morphology of chromium deposits on mild-steel substrate was examined under a scanning electron microscopy (SEM). In Figs. 1A and B and 2A and B, the surface structure of pure chromium from Cr(III) and Cr(VI)-baths under scanning microscope is compared. Fig 1A and B are the SEM photomicrographs of DC electrodeposited chromium at 35 A/dm^{-2} for 30 min from Cr(III) and Cr(VI)-baths, respectively. Both deposits have a small nodular deposit with the particle size of about 2–2.5 μm with micro cracks.
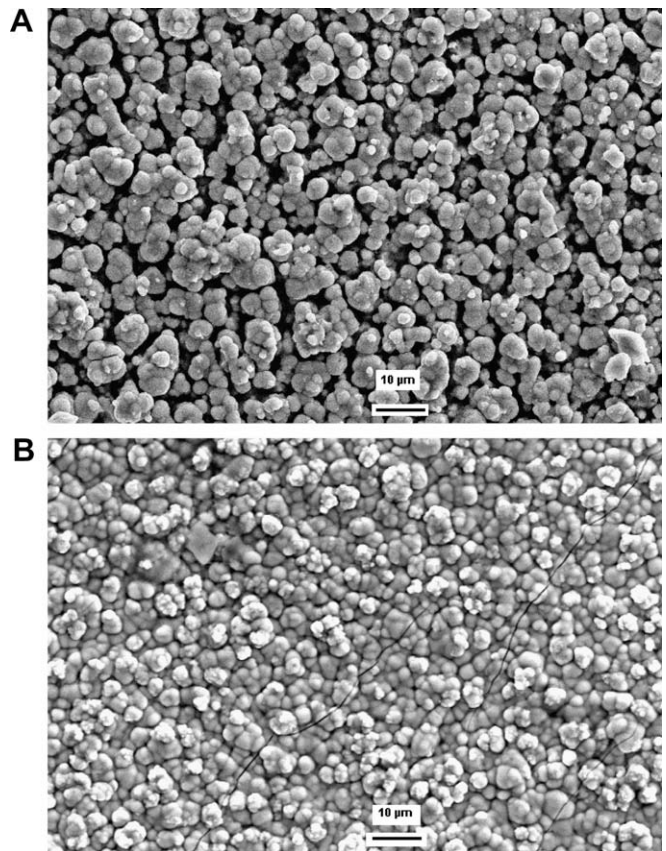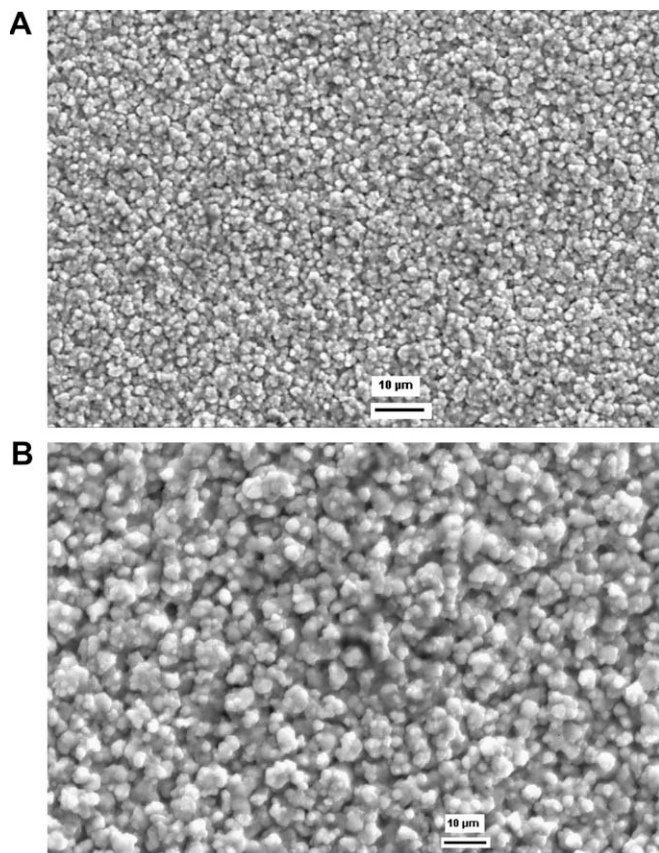

Fig. 1. (A and B) SEM surface morphology of DC-deposited chromium at 35 A/dm^2 in 30 min from Cr(III) and Cr(VI)-baths.

The micro cracks formed during electrodeposition is due to the adsorbed hydrogen gas. Similarly, Fig. 2A and B is the SEM photomicrographs of PE-deposited chromium at an average current density of 10.4 A/dm^2 for Cr(III) both and 20 A/dm^2 for Cr(VI)-bath in 30 min. Both the deposits have a very small nodular size with the particle size of about 1–1.4 μm. In the PE deposition, the peak current density is higher than average current density, this leads to a decreased grain size. The decreased porosity and denser packed surface are due to the desorption of hydrogen during the off time of pulse cycle [14].

3.2. X-ray diffraction analysis

Chromium may be electrodeposited in various phases (α-, β- and γ-phase) [15]. The phases obtained are dependent on plating conditions. α-Chromium [16,17] is the most predominant and stable phases; however, β-chromium only deposits under certain conditions and converts eventually to α-chromium over time or with annealing. Fig. 3 shows the X-ray diffraction pattern of the chromium deposited from hexavalent and trivalent chromium baths. The α-Cr(110) was peak obtained at $2\theta = 44.6992$ and $2\theta = 44.2276$ from trivalent and hexavalent chromium baths respectively. Similarly, α-Cr(200) peaks were obtained at $2\theta = 65.0869$ and $2\theta = 64.7460$ from trivalent and hexavalent chromium baths, respectively. Intensity of α-Cr(110) peak is higher in trivalent, whereas α-Cr(200) peak is higher in hexavalent chromium. The α-Cr(110) plane is having higher intensity in BCC structure from trivalent bath. Therefore, the α-Cr deposits tend to grow with the plane of highest intensity. In contrast to α-Cr(110), the preferred orientation in hexavalent chromium bath is α-Cr(200). The crystallite sizes of Cr coatings were calculated from Scherer's equation.

Fig. 2. (A and B) SEM surface morphology of PE-deposited chromium at an average current density was 10.4 A/dm^2 and 20 A/dm^2 from Cr(III) and Cr(VI)-baths in 30 min.
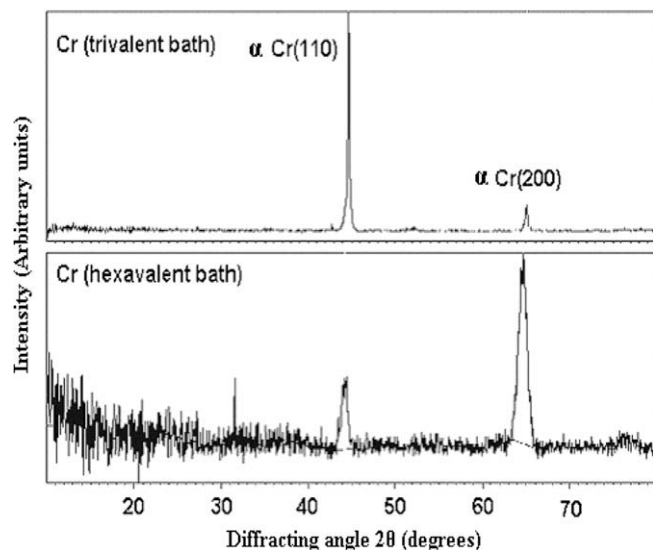
Fig. 3. XRD pattern of chromium coatings from Cr(III) and Cr(VI)-baths.

The values of texture coefficient $T_C[ø]$ and grain size are tabulated in Table 2A and B.

$$D = \frac{0.94\lambda}{\beta \cos\theta} \qquad (1)$$

where D is the grain size, β is the full width at half maximum (FWHM) of the diffraction peak, λ is the wavelength of the inciden-

Table 2

(A and B) Texture coefficient and crystallite size of Cr from trivalent and hexavalent baths obtained from XRD pattern.

hkl (Trivalent bath)	2θ	D [Å]	I/I_O	$T_C[ø]$	Crystallite size (nm)
A					
α-Cr(1 1 0)	44.6992	2.02741	1	65.08	71.33
α-Cr(2 0 0)	65.0869	1.43195	0.5365	34.91	32.08
B					
α-Cr(1 1 0)	44.2276	2.04793	0.3825	7.10	11.86
α-Cr(2 0 0)	64.7460	1.43866	5	92.89	10.67

tal X-ray (1.54 Å), and θ is the diffraction angle. Based on Eq. (1), the average crystallite sizes were found to be 71.33 α-Cr(1 1 0) and 32.08 nm α-Cr(2 0 0) in trivalent chromium bath. Similarly, the average crystallite sizes were found to be 11.86 α-Cr(1 1 0) and 10.67 nm α-Cr(2 0 0) in hexavalent chromium bath, respectively.

The preferred growth orientation was determined using texture coefficient TC_{hkl}. This factor can be calculated by using

$$TC_{hkl} = \frac{I/I_0}{1/N\left\{\sum[I/I_0]\right\}}$$

where TC_{hkl} is the texture coefficient of the plane, I_{hkl} is the measured intensity of the $(h k l)$ plane, $I_{0(hkl)}$ corresponds to the recorded intensity in the JCPDS data file and N is the number of preferred directions of the growth. The TC_{110} was found to be 65.08 and 92.89 from trivalent and hexavalent chromium baths.

3.3. Corrosion examinations

3.3.1. Potentiodynamic polarization tests

Fig. 4 shows potentiodynamic polarization curves for electrodeposited chromium in 3.5%NaCl solution. All the curves display the active passive behavior between −0.9 and −0.2 V. It indicates that the mechanism of activity and passivation is similar in essence for all electrodeposits. The current density increases with the increasing potential at the activation region. And then the electrode passivates and displays high stability, as characterized by the low and steady value of passive current density. The corrosion current density (I_{corr}) and corrosion potential (E_{corr}) are calculated from the intercept of the Tafel slopes. The corrosion rate (CR) in mils per year was estimated from the polarization curves, and is given in Table 3. Among all the samples, Cr-(PED)/MS from Cr(VI)-bath and Cr-(PED)/MS from Cr(III)-bath exhibit the lowest values of I_{corr} and CR than that of samples Cr-(DCD)/MS and mild steel (MS). From the values, sample Cr-(PED)/MS from Cr(III)-bath has the smaller differences of I_{corr} and CR than that of Cr-(PED)/MS from Cr(VI)-bath. Therefore, PE-deposited chromium from Cr(III)-bath is suitable to replace carcinogenic, non eco-friendly Cr(VI)-bath, which is attributed to the compact microstructure.

3.3.2. Electrochemical impedance spectra tests

The measured impedance spectra for the electrodeposits in 3.5%NaCl solution are shown as Bode and Nyquist diagrams in Fig. 5B and C. The impedance plots exhibit depressed semicircles. The equivalent circuit as shown in Fig. 6 is used to fit the corrosion resistance parameters. R_{ct} and C_{dl} represent the charge-transfer resistance and double layer capacitance, respectively. The fitted impedance spectra are in good agreement with the impedance spectra recorded during the measurements as shown in Fig. 5. The calculated values of circuit elements are listed in Table 4. It can be found that all fitted corrosion parameters of the electrodeposits vary with the changes of the microstructure. The corrosion resistance (R_{ct}) of Cr-(PED)/MS from Cr(III)-bath and Cr-(PED)/MS
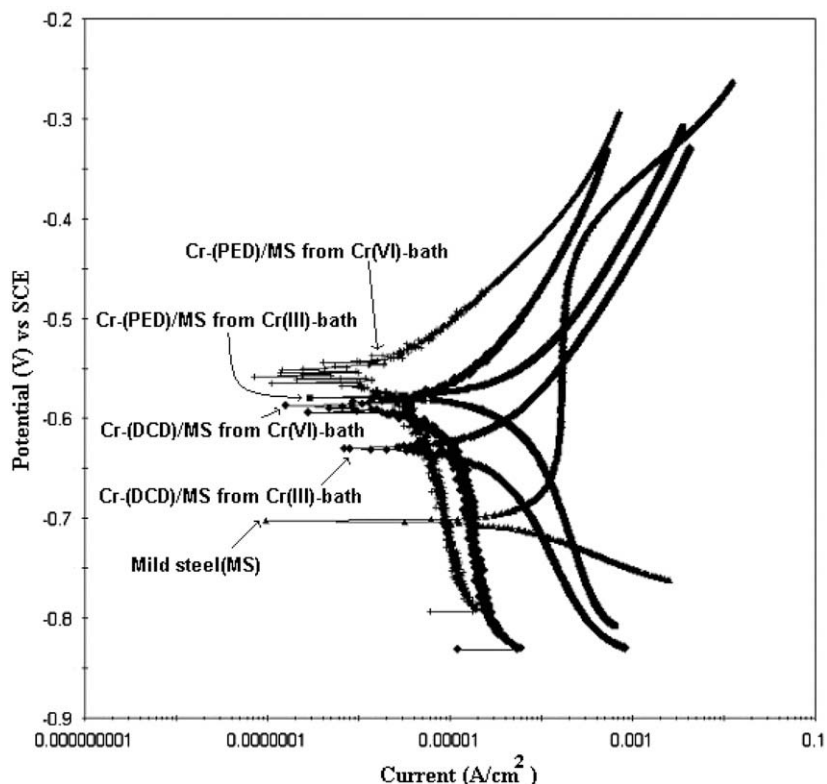
Fig. 4. Polarization studies of MS panel, Cr on MS (DCD) and Cr on MS (PED) from Cr(III) and Cr(VI)-baths in 3.5% w/v NaCl electrolyte.

Table 3
Corrosion parameters obtained from polarization studies in 3.5% w/v NaCl electrolyte.

Sample	E_{corr} vs SCE (mV)	b_a (V/decade)	b_c (V/decade)	I_{corr} (A/cm^2)	Corrosion rate (mpy)
MS panel	−0.702	0.483	−0.043	8.47×10^1	3.91×10^1
Cr on MS (DCD) Cr(III)-bath	−0.629	0.150	−0.225	5.01×10^1	1.56×10^1
Cr on MS (PED) Cr(III)-bath	−0.588	0.182	−0.421	2.70×10^1	8.43
Cr on MS (DCD) Cr(VI)-bath	−0.619	0.555	−0.302	3.41×10^1	1.04×10^1
Cr on MS (PED) Cr(VI)-bath	−0.556	0.112	−0.495	4.8	1.50

from Cr(VI)-bath have higher values than that of DC-deposited chromium and mild steel (MS). The increased R_{ct} values and decreased C_{dl} values for Cr deposits clearly confirm the better corrosion resistance of these Cr-(PED)/MS from Cr(III)-bath than that of DC deposited and bare mild steel as observed from the high frequency region of the impedance spectra.

3.3.3. Porosity of DC and PE-deposited systems

It is possible to determine the porosity of a coating using an electrochemical measurement technique that determines the ratio of the current density through the pores and the coating [18]. Using the facts that when determining the porosity, in most cases the cathodic current is negligible, and the current density is inversely proportional to the polarization resistance. Elsener et al. [19] estimated the porosity of TiN-coated mild steel from the shift of the corrosion potential caused by the presence of the coating (ΔE_{corr}) and from the individual polarization resistance of the coatings (R_p) and the substrate materials ($R_{p,s}$) as given below

$$P = \left(\frac{R_{p,s}}{R_p}\right) \times 10^{-|\Delta E_{CORR}|/b_a}$$

where b_a is the Tafel slope of the active dissolution of mild steel.

Using this equation, and the values of ($R_{p,s}$) (63 Ω cm^2) and b_a (0.483 V/decade) determined from the separate measurement on an uncoated mild-steel (MS) substrate in 3.5%Nacl solution, we estimate the porosity of the Cr-(DCD)/MS from Cr(VI)-bath, Cr-(PED)/MS from Cr(VI)-bath, Cr-(DCD)/MS from Cr(III)-bath and Cr-(PED)/MS from Cr(III)-bath systems. For this purpose, the E_{corr} of the mild steel was determined to be −702 mV vs SCE. The coating porosity determined in this way is given in Table 4.

From these values, Cr-(PED)/MS from Cr(III)-bath (P = 0.013%) differs only 1.5 times of Cr-(PED)/MS from Cr(VI)-bath (P = 0.00813%). Therefore, PE-deposited chromium from the Cr(III)-bath is having better corrosion resistance and a good choice to replace conventional hexavalent chromium plating process.

4. Conclusions

Eco-friendly Cr(III)-glycine-based electrolyte was developed, from which microstructure and electrochemical corrosion behavior of DCD and PED Cr coating were studied and compared to the microstructure and electrochemical corrosion behavior of Cr coating from Cr(VI)-bath.
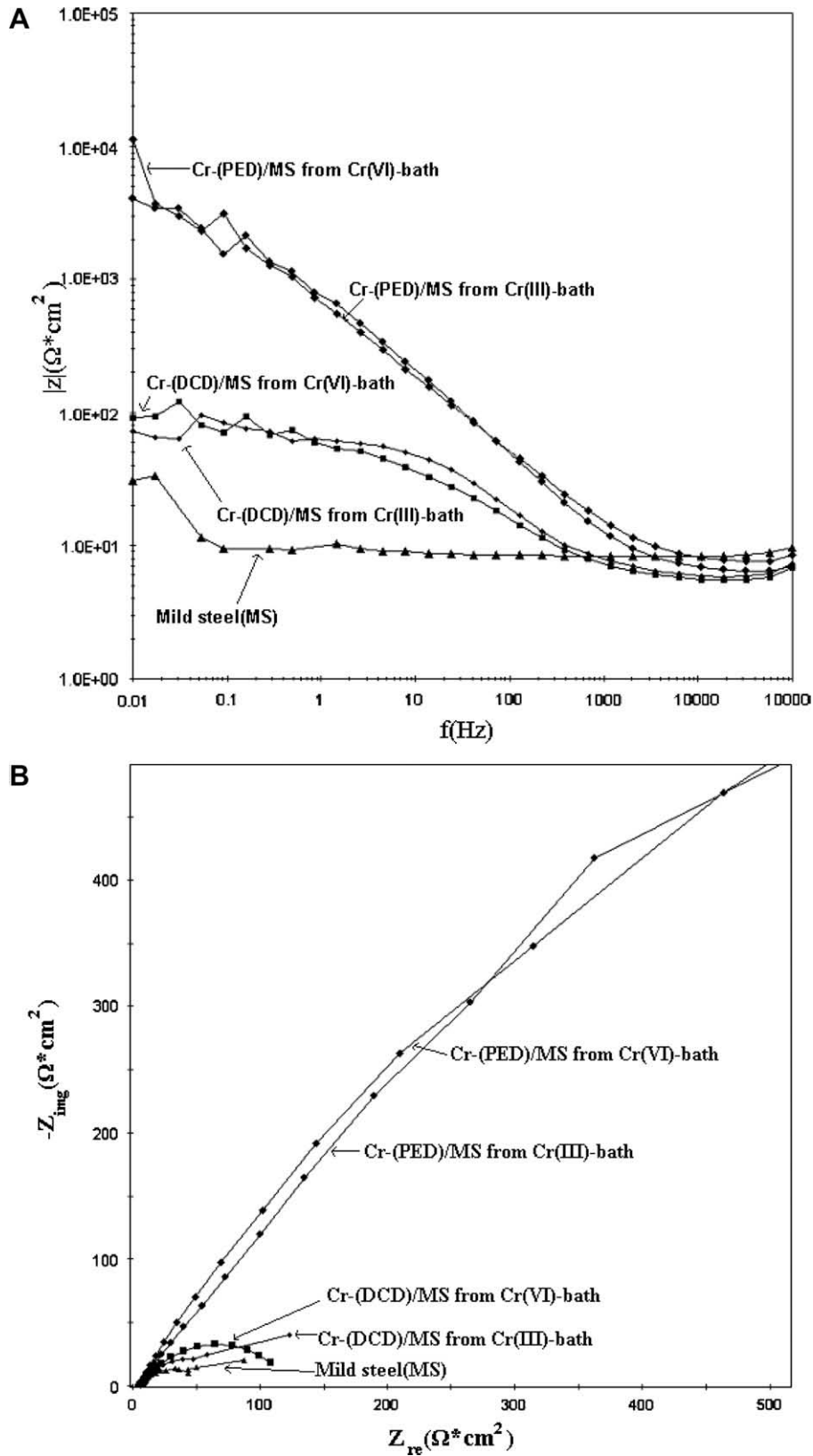
Fig. 5. Impedance spectra of MS panel, Cr on MS (DCD) and Cr on MS (PED) from Cr(III) and Cr(VI)-baths: (A) Bode–Bode plot; (B) Nyquist plot.

1. Using potentiodynamic test, the current density of DC and PE-deposited coated, uncoated substrate and the differences in their corrosion potentials (E_{corr}) were determined. In all the cases, the (E_{corr}) shifted to a more positive potential when the coatings were applied. The PE-deposited substrate had a better corrosion resistance than DC and mild-steel substrate. Corro-
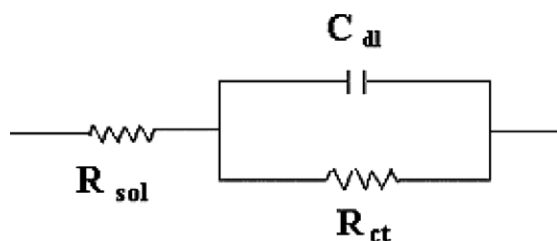
Fig. 6. Equivalent circuit diagram of impedance spectra for electrodeposited chromium in 3.5%NaCl electrolyte.

Table 4
Corrosion parameters and porosity obtained from impedance measurements by Nyquist plots.

Sample	OCP (V)	R_{ct} * (Ω cm^2)	C_{dl} (F/cm^2)	Porosity (%)
MS panel	−0.511	63	8.75×10^{-4}	–
Cr on MS (DCD) Cr(III)-bath	−0.580	111.5	6.78×10^{-2}	0.399
Cr on MS (PED) Cr(III)-bath	−0.582	2807	5.44×10^{-4}	0.013
Cr on MS (DCD) Cr(VI)-bath	−0.597	116.9	12.21×10^{-2}	0.362
Cr on MS (PED) Cr(VI)-bath	−0.543	3860	7.03×10^{-4}	0.0081

sion properties of PE-deposited chromium from Cr(III)-bath differ only 1.5 times (higher positive potential, lower current density (I_{corr}) and lower corrosion rate) than that of PE deposited chromium from Cr(VI)-bath.

2. EIS data for DC and PE-deposited chromium from Cr(III) and Cr(VI)-baths showed that the values of charge-transferred resistance (R_{ct}) and double layer capacitance (C_{dl}) of PE deposited from Cr(III) bath were not much different from those of Cr(VI)-bath.

3. The porosities of both DC and PE-deposited chromium on the mild-steel substrate from Cr(III) and Cr(VI)-baths were quanti-tatively estimated. Among the porosity values, PE deposited chromium from Cr(III)-bath differs only 1.5 times. Therefore, the structure and corrosion properties of PE-deposited chromium from Cr(III)-bath are comparable to those of Cr(VI)-bath. So developed trivalent chromium coatings are very good choice to replace toxic, carcinogenic Cr(VI)-bath by Cr(III)-bath.

Acknowledgment

References

[1] A. Lozano-Morales, R.P. Renz, J.J. Fortman, E.J. Taylor, ECS Trans. 6 (9) (2007) 51–61.
[2] Zhixiang Zeng, Junyan Zhang, Surf. Coat. Technol. 202 (12) (2008) 2725–2730.
[3] Kee-Seok Nam, Ku-Hyun Lee, Shik-Cheol Kwon, Deuk Yong Lee, Yo-Seung Song, Mater. Lett. 58 (2004) 3540–3544.
[4] Sik-Chol Kwon, Halk-Jun Lee, Jong-Kuk Kim, Eungsun Byon, George Collins, Ken Short, Surf. Coat. Technol. 201 (15) (2007) 6601–6605.
[5] B. Li, A. Lin, F. Gan, Surf. Coat. Technol. 201 (6) (2006) 2578–2586.
[6] S.K. Ibrahim, D.T. Gawne, A. Watson, Trans. Inst. Metal. Finish. 76 (4) (1998) 156–161.
[7] S. Surviliene, V. Jasulaitiene, O. Nivinskiene, A. Cesuniene, Appl. Surface Sci. 253 (16) (2007) 6738–6743.
[8] J.-Y. Hwang, Plat. Surf. Finish. 78 (5) (1991) 118–124.
[9] M. El-Sharif, S. Ma, C.U. Chisholm, Trans. Inst. Metal. Finish. 77 (4) (1999) 139–144.
[10] Y.B. Song, D.-T. Chin, Electrochim. Acta 48 (4) (2002) 349–356.
[11] N.V. Mandich, Plat. Surf. Finish. 84 (5) (1997) 108–115.
[12] M. El-Sharif, C.U. Chisholm, Trans. Inst. Met. Finish. 75 (6) (1997) 208–212.
[13] G. Devaraj, S.K. Seshadri, Plat. Surf. Finish. 83 (6) (1996) 62–66.
[14] Kenneth Haug, Timothy Jenkins, J. Phys. Chem. B 104 (2000) 10017–10023.
[15] H. Dasarathy, C. Riley, H.D. Coble, J. Electrochem. Soc. 141 (1994) 1773–1779.
[16] Daniel Sherwood, Bosco Emmanuel, Cryst. Growth Des. 6 (2006) 1415–1419.
[17] Hideya Okada, Takeo Ishida, Nature 187 (1960) 496–497.
[18] W. Tato, D. Landolt, J. Electrochem. Soc. 145 (1998) 4173–4181.
[19] B. Elsener, A. Rota, H. Bohni, Mater. Sci. Forum. 29 (1989) 44–45.